Front. Earth Sci.
https://doi.org/10.1007/s11707-024-1142-x

RESEARCH ARTICLE

Projected changes in rare extreme precipitation design values in the United States due to global warming

Kenneth E. KUNKEL (✉), Xia SUN, Liqiang SUN

North Carolina Institute for Climate Studies, North Carolina State University, Asheville, NC 28801, USA

Abstract There is high confidence that extreme precipitation will increase in most areas if the globe continues to warm. In the US, NOAA Atlas 14 (NA14) is the most authoritative source for heavy rainfall frequency values used in infrastructure planning and design. However, NA14 assumes a stationary climate and uses only historical observations to estimate values. Thus, use of such values for design may lead to underperformance of long-lived infrastructure, thereby placing people and property at increased risk from flooding. Analyses of global climate model (GCM) simulations suggest that projected extreme precipitation changes will be positive nearly everywhere in the US and will be larger for shorter durations, lower annual exceedance probabilities (AEPs), and higher emissions. Herein, we provide adjustment factors that can be applied to observations-based precipitation frequency values to estimate potential future changes under selected global warming levels. These are derived from two statistically downscaled daily precipitation datasets (STAR and LOCA2) developed using modern methods that focus in part on modeling the high tail of the precipitation distribution with a high degree of fidelity. These datasets, each consisting of 16 ensemble members downscaled from a common set of 16 CMIP6 GCMs, provide estimates for durations of daily and longer. The set of adjustment factors are extended using seven models from the NA-CORDEX suite of dynamically downscaled simulations by analyzing the change in adjustment factors from daily to hourly durations. There is an average increase in the adjustment factors of about 1.3. This factor is applied to the daily adjustment factors from STAR and LOCA2 to produce estimates for the hourly duration.

Keywords precipitation, extremes, climate, projections

Received May 31, 2024; accepted December 19, 2024

E-mail: kekunkel@ncsu.edu

1 Introduction

Global warming from increasing atmospheric concentrations of greenhouse gases is projected to cause increases in extreme precipitation in most areas of the globe (Seneviratne et al., 2021). There is a high confidence in these projections because one dimension of the underlying physics is quite simple. Extreme precipitation amounts are highly correlated with atmospheric water vapor content (AWVC). The saturated value of AWVC is a highly nonlinear function of temperature, increasing by 6%–7% $°C^{-1}$ according to a relationship known as Clausius–Clapeyron (C-C). Thus, changes in temperature will lead to increases in saturated AWVC, which in turn increases the potential for heavy precipitation. However, there are other factors that influence extreme precipitation, which can affect the local magnitude and even the sign of change, some of which are addressed in Section 2.

The potential adverse impacts of flooding caused by extreme precipitation can be partially mitigated by the climate-aware design of infrastructure that handles runoff and by policies and regulations on development. The most prominent and widely used source of such information in the US is NOAA Atlas 14 (NA14; e.g., Bonnin et al., 2006a, 2006b, 2006c). Its 11 volumes provide precipitation frequency values for a wide range of event durations (5 min to 60 days) and average recurrence intervals (1 to 1000 years) for most areas of the US.

The rainfall frequency values in NA14 are estimated from analyses of precipitation observations at thousands of stations. These analyzed stations represent a wide range of periods of record, from a few years to more than 100 years. The analyses assume that the climate is stationary. However, numerous research studies have found that the frequency and intensity of extreme precipitation has been increasing (DeGaetano and Castellano, 2017; Kunkel et al., 2020a; Nazarian et al., 2022; Marvel et al., 2023), and the more rapid

intensification of more extreme events appears as a robust feature at finer regional scales (Li et al., 2019). Given that any future warming is projected to add further increases to extreme precipitation, the NA14 values are likely underestimates of the potential future values (Wright et al., 2019). Thus, the current use of these values for long-term design and planning may lead to underperformance of long-lived infrastructure, thereby placing people and property at increased risk from flooding (Wright et al., 2021).

The development of heavy rainfall projections suitable for infrastructure design and resilience planning poses several scientific challenges. The purpose of this paper is to describe and frame these challenges and to present the results of analyses that can be applied to accommodate future climate change for the coterminous United States.

2 Challenges and limitations

A first-order assumption is that warming will increase AWVC following the C-C relationship and extreme precipitation will increase in proportion. However, the processes determining the quantitative scaling of extreme precipitation are complex and this has been, and continues to be, the subject of extensive theoretical, modeling, and observational investigations (e.g., O'Gorman, 2015; Kunkel et al., 2020b; NASEM, 2024). Conceptually, the scaling is affected by both thermodynamic and dynamic effects. The thermodynamic component is typically considered to be the change in AWVC while the dynamic component represents circulation changes that affect convergence and vertical motion. However, Neelin et al. (2022) point out that the thermodynamic energy budget equation must also be satisfied when AWVC changes and that changes in convergence and vertical velocity may be required to meet the dual constraints of the moisture and energy budgets. Thus, extreme precipitation scaling can deviate from the C-C 6%–7% $°C^{-1}$ from AWVC changes alone.

In the extratropics, the geographic focus of this study, O'Gorman and Schneider (2009) showed that climate models increase the 99.9th percentile of daily precipitation at about the rate of the moist-adiabatic derivative of saturation specific humidity, which is smaller than the saturation specific humidity. O'Gorman (2015) further elaborated on the potential influence of warming on extratropical cyclones (ETCs), considered in the context of the quasi-geostrophic omega equation (Holton, 1992). In this framework, upward vertical motion is diagnostically related to differential positive vorticity advection and warm air advection. O'Gorman (2015) concluded that large-scale changes in vertical motion from warming are likely to be small because of the dominating effect of planetary rotation compared to static stability. This is relevant because most of the daily extreme precipitation events within the continental US (CONUS) are caused by ETCs and their accompanying fronts (Kunkel et al., 2012). However, at short durations, the importance of convective processes likely increases. For example, Förster and Thiele (2020) analyzed historical observed and modeled precipitation for selected stations in Europe and found much larger scaling factors for hourly extremes compared to daily extremes. Convection-permitting climate model simulations generally project extreme sub-daily precipitation increases at scaling rates of C-C or higher (Seneviratne et al., 2021). A convection-permitting simulation over CONUS (Prein et al., 2017) found that the scaling for hourly extremes exceeds that for daily extremes. Furthermore, O'Gorman and Schneider (2009) point out that the investigation of scaling relationships should examine the days when extreme precipitation occur. Temperature changes on those days may differ from overall mean changes. These and many other studies illustrate that the quantitative relationship between future global warming and extreme precipitation is uncertain and will likely vary by location, event duration, and event rarity, at a minimum.

Analysis of future changes in climate conditions relies heavily on global climate model (GCM) simulation data, particularly from the various phases in the Coupled Model Intercomparison Project (CMIP). The latest phase (CMIP6) includes simulations covering historical and future periods from several dozen climate models. The ready availability of these data (see Section 3) facilitates a range of analyses in support of extreme precipitation research.

The analyses herein address the need for extreme precipitation design values, incorporating future global warming, in the coterminous US for a range of durations from hourly to 10 days and for a range of annual exceedance probabilities (AEPs) from 0.5 to 0.01 using a combination of statistically-downscaled and dynamically-downscaled datasets.

3 Data and methods

Observations of daily precipitation were obtained from the Global Historical Climatology Network-Daily (GHCN-D) dataset. Data were obtained for US stations with less than 10% missing daily observations for the period of 1951–2023. A total of 3110 stations within the coterminous US were identified and analyzed.

Daily precipitation and 2 m specific humidity data from 39 CMIP6 models were used for analyses (Table 1). These data were from the historical and future scenarios (ScenarioMIP) experiments (Eyring et al., 2016; O'Neill et al., 2016). Not all of these 39 models were available for each variable and each scenario. The analyses included all models available for a given variable and scenario. All

Table 1 Models used in Figs. 2–6, as indicated by "×". Asterisks indicate common models for which both LOCA2 and STAR downscaled data were available

Model	Precip SSP2-4.5	Precip SSP3-7.0	Precip SSP5-8.5	Sp Hum SSP2-4.5	Sp Hum SSP3-7.0	Sp Hum SSP5-8.5
ACCESS-CM2*	×	×	×	×	×	×
ACCESS-ESM1-5*	×	×	×	×	×	×
BCC-CSM2-MR*	×	×	×	×	×	×
CAMS-CSM1-0	×	×	×			
CESM2	×	×	×	×	×	×
CESM2-WACCM	×	×	×	×	×	×
CMCC-CM2-SR5	×	×	×	×	×	×
CMCC-ESM2	×	×	×	×	×	×
CNRM-CM6-1	×	×	×	×	×	×
CNRM-CM6-1-HR			×	×	×	×
CNRM-ESM2-1		×	×	×	×	×
CanESM5*	×	×	×	×	×	×
EC-Earth3*	×	×	×	×	×	×
EC-Earth3-AerChem		×			×	
EC-Earth3-CC	×		×	×		×
EC-Earth3-Veg	×	×	×	×	×	×
EC-Earth3-Veg-LR	×	×	×	×	×	×
FGOALS-g3*	×	×	×	×		
GFDL-CM4	×		×	×		×
GFDL-ESM4*	×	×	×	×	×	×
HadGEM3-GC31-LL	×		×	×		×
HadGEM3-GC31-MM			×			×
IITM-ESM	×	×	×	×	×	×
INM-CM4-8*	×	×	×	×	×	×
INM-CM5-0*	×	×	×	×	×	×
IPSL-CM5A2-INCA		×				
IPSL-CM6A-LR*	×	×	×			
KACE-1-0-G	×	×	×	×	×	×
KIOST-ESM	×		×			
MIROC-ES2L	×	×	×	×		
MIROC6*	×	×	×			
MPI-ESM1-2-HR*	×	×	×	×	×	×
MPI-ESM1-2-LR*	×	×	×	×	×	×
MRI-ESM2-0*	×	×	×	×	×	×
NESM3	×		×			
NorESM2-LM*	×	×	×	×	×	×
NorESM2-MM*	×	×	×	×	×	×
TaiESM1	×		×	×		×
UKESM1-0-LL	×	×	×	×	×	×

computations were done on the Amazon Web Services cloud, accessing their archive of CMIP6 data.

Two statistically downscaled datasets were used: the Localized Constructed Analogues, version 2 (LOCA2; Pierce et al., 2023) and the Seasonal Trends and Analysis of Residuals (STAR; Hayhoe et al., 2024). Both of these datasets include daily precipitation, daily maximum temperature, and daily minimum temperature for the period 1950–2100 for the SSP2-4.5 and SSP5-8.5 scenarios. Both cover the coterminous United States, at

1/16° resolution for LOCA2 and 1/24° resolution for STAR. Analyses herein included downscaled data from 16 CMIP6 GCMs that were common to both downscaled datasets (Table 1). These two datasets were used in the Fifth National Climate Assessment (Basile et al., 2023). Both of these methods model the high tail of the daily precipitation with increased fidelity compared to previous methods (Pierce et al., 2023; Hayhoe et al., 2024), making these datasets good candidates for design applications using extreme precipitation frequency levels.

The North American Coordinated Regional Downscaling Experiment (NA-CORDEX) has gathered data from regional climate model simulations covering a domain representing most of North America. Data for a set of 7 simulations (Table 2) covering a common period of 1970–2099 at a spatial resolution of 25 km were obtained for this study. These simulations used historical forcing through 2005. For 2006–2099, forcing for the RCP8.5 emissions scenario was used.

Two approaches were used to analyze future projections. In one approach, differences between 30-yr block averages were computed for selected future SSP projections for individual models, and then combined into multi-model statistics. In the second approach, differences were calculated for selected Global Warming Levels (GWL) relative to preindustrial conditions, and then combined into multi-model statistics. The GWL approach was used widely in the Intergovernmental Panel on Climate Change's Sixth Assessment Report (IPCC, 2021) and the US Fifth National Climate Assessment (USGCRP, 2023).

Precipitation return levels were calculated from the downscaled datasets using non-stationary Generalized Extreme Value (GEV) analysis with GWL as the non-stationary covariate. The non-stationary GEV probability distribution function is defined as:

$$f(x,t) = \frac{1}{\sigma(x,\mathrm{GWL})}\left\{1+\xi(x)\frac{x-\mu(x,\mathrm{GWL})}{\sigma(x,\mathrm{GWL})}\right\}^{\left(-\frac{1}{\xi(x)}-1\right)} \times \exp\left(-\left\{1+\xi(x)\frac{x-\mu(x,\mathrm{GWL})}{\sigma(x,\mathrm{GWL})}\right\}^{-\frac{1}{\xi(x)}}\right), \quad (1)$$

where μ, σ, and ξ are location, scale and shape distribution parameters, respectively, x is the spatial coordinate (model grid point), and GWL represents global warming level (K) with respect to pre-industrial conditions. Location and scale parameters (Eqs. (2) and (3), respectively) were allowed to vary with the temporal covariate (GWL). Because of its sensitivity to outliers, the shape coefficient was held constant (Eq. (4)) to avoid the generation of unreasonable values when modeling through time (OWP, 2022). For each model grid point, the parameters are defined as follows:

$$\mu(x,\mathrm{GWL}) = a_0 + a_1 \times \mathrm{GWL}\,, \quad (2)$$

$$\ln[\sigma(x,\mathrm{GWL})] = b_0 + b_1 \times \mathrm{GWL}\,, \quad (3)$$

$$\xi(x) = c_0\,. \quad (4)$$

Precipitation threshold values, z_{AEP}, for a specified fraction of annual exceedance probability, AEP, is calculated as

$$z_{\mathrm{AEP}} = \mu - \frac{\sigma}{\xi}\left[1-\{-\log(1-\mathrm{AEP})\}^{\xi}\right]. \quad (5)$$

4 Results

Historical trends provide a context for changes that will be imposed by future warming. Annual maximum series for 1951–2023 were constructed for the 3110 GHCN-D stations. Linear least squares analysis with time as the independent variable was applied to each time series and the slope was tested for statistical significance based on the false discovery rate (FDR) procedure described in Wilks (2016). The results of this analysis (Fig. 1) indicate a mix of statistically significant upward and downward trends, with a majority of stations having non-significant trends. At stations experiencing statistically significant trends, most were upward. Of the 3110 stations, 58 (10) show statistically significant upward (downward) trends. This preponderance of upward trends is most prominent in the eastern US, whereas there is a more even mix in the western US. The east–west contrast in trends is a known feature of extreme precipitation in the US (e.g., Marvel et al., 2023).

A similar trend analysis was applied to the daily grid point precipitation from 37 CMIP6 models for the period

Table 2 NA-CORDEX models used in this paper along with the simulation period. The column headings indicate the name of the CMIP5-driving GCM. The year that these models reach the 3°C global warming level is listed in the second row. The row headings indicate the name of the regional climate model

	GFDL-ESM2M	MPI-ESM-LR	HadGEM2-ES	NorESM1-M
Global Warming Level: 3°C	2083	2063	2060	2078
WRF (Weather Research and Forecasting)	1950–2099	1950–2099	1950–2099	
REMO (REgional MOdel)		1970–2100	1970–2099	1970–2100
RegCM4 (Regional Climate Model version 4)		1949–2100		

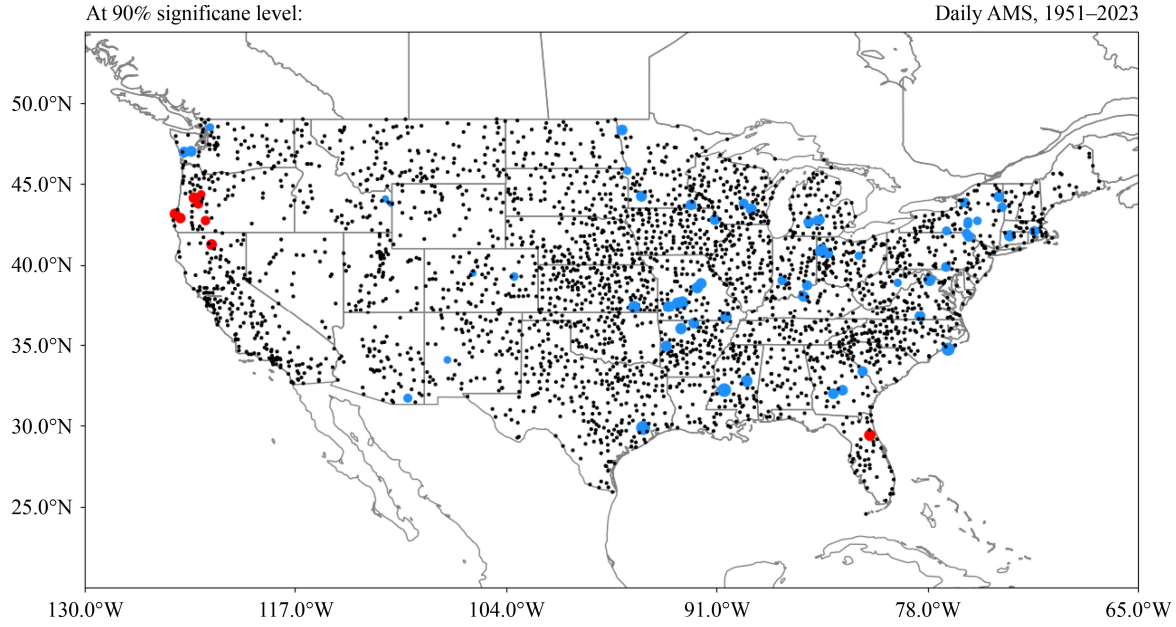

Fig. 1 Linear least-squares trend in Annual Maximum Series for 1951–2023 for selected stations from Global Historical Climatology Network-Daily. Blue (red) circles indicate stations with statistically significant (global α = 0.10) upward (downward) trends. Black circles indicate stations with non-statistically significant trends.

1951–2023. Annual Maximum Series (AMS) were constructed for this period from the concatenation of the historical simulation period of 1951–2014 with the SSP5-8.5 ScenarioMIP simulation for 2015–2023. For CMIP6 models with multiple ensemble members, only the first ensemble member was analyzed. The multi-model mean (MMM) trends (Fig. 2, top panel) indicate upward trends over most of the globe, with exceptions in some oceanic subtropical areas where the multi-model mean is downward.

The fraction of models with nominal upward trends was calculated (Fig. 2, bottom panel). This fraction is less than 1.0 nearly everywhere, indicating that grid point trends are downward for some individual ensemble members. A closer examination of this feature over the coterminous US and adjacent regions is shown in Fig. 3. The MMM trend (Fig. 3, top panel) is upward everywhere over the coterminous US, in the range of 0–10% change over the 73-yr period of analysis. The 10% and 90% confidence limits were estimated from the trend standard deviation assuming a normal distribution. The 10% confidence limits (Fig. 3, middle panel) are downward everywhere, as much as around a 20% downward change. By contrast, the 90% confidence limits are strongly positive, with a change as large as +25%. Overall, the Fig. 3 results indicate that the range of grid point trends across the 37 models is large compared to the MMM trend.

Climate model simulation of projected changes was analyzed by examining block averages over 30-yr periods between historical and future (ScenarioMIP) experiments for the periods of 1985–2014 and 2070–2099, respectively. Two metrics were used: the AMS and the 30-yr daily maximum. Future changes were computed for the SSP2-4.5, SSP3-7.0, and SSP5-8.5 scenarios. Two climate variables were analyzed: specific humidity at 2 m and precipitation.

Douville et al. (2021) showed that the global mean annual precipitable water increases by 15.2%, 25.0%, and 31.9% for SSP2-4.5, SSP3-7.0, and SSP5-8.5, respectively by the end of the 21st Century (2081–2100) with respect to 1995–2014. Figure 4 shows simulated future changes in extreme metrics of 2 m specific humidity. There are increases everywhere for all three scenarios and both metrics. This reflects the C-C constraint on high values of water vapor content. Temperature increases occur everywhere in these simulations, and water vapor content also increases as temperature increases. The magnitude of the changes increases as the forcing increases from SSP2-4.5 to SSP5-8.5. Also, the increases are somewhat higher for the 30-yr maximum than for the annual maximum. The magnitudes of the global average increases are 11.4% (13.2%), 16.9% (19.5%), and 22.4% (25.6%) for the annual daily maximum (30-yr daily maximum) for SSP2-4.5, SSP3-7.0, and SSP5-8.5, respectively by the end of the 21st Century (2070–2099) with respect to 1985–2014. These values for 2 m specific humidity are slightly smaller than the Douville et al. (2021) results for precipitable water.

Figure 5 shows the results for daily precipitation. The general patterns are similar for all combinations of scenario and metric. There are increases everywhere, except for decreases in some oceanic subtropical areas. The magnitude of both increases and decreases becomes larger as forcing increases from SSP2-4.5 to SSP5-8.5. The magnitude of increases is larger for the 30-yr

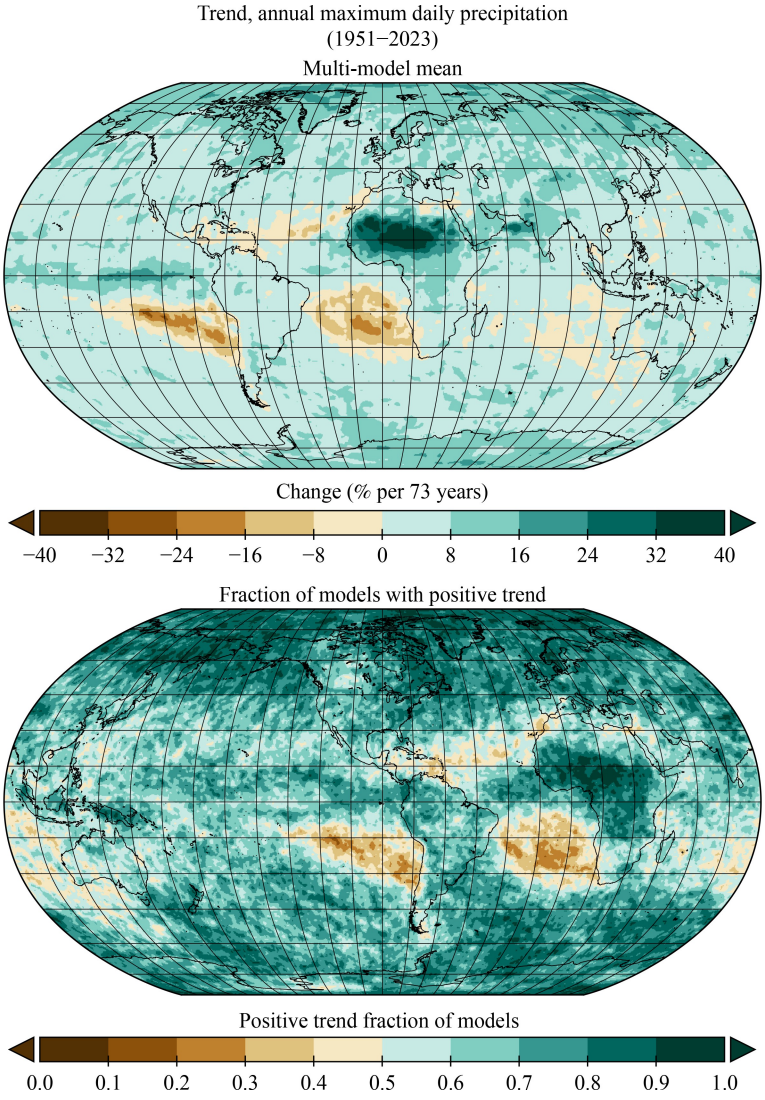

Fig. 2 Statistics of the multi-model mean (MMM) trend in the Annual Maximum Series for 1951–2023 from 37 CMIP6 GCMs. Top panel indicates MMM trend magnitude in units of percent change over the 73-yr period of analysis. Bottom panel indicates the fraction of models with a nominal upward trend.

maximum than the annual maximum, while the magnitude of decreases in the scattered oceanic subtropical regions is larger for annual maximum than for the 30-yr maximum. The magnitudes of the global average increases are 8.0% (15.8%), 11.1% (21.3%), and 15.8% (28.1%) for the annual daily maximum (30-yr daily maximum) for SSP2-4.5, SSP3-7.0, and SSP5-8.5, respectively by the end of the 21st Century (2070–2099) with respect to 1985–2014. The changes in annual maximum (30-yr maximum) precipitation are somewhat smaller (larger) than the corresponding changes in extreme 2 m specific humidity. Seneviratne et al. (2021) present projections of the AMS for several global warming levels. These show similar spatial patterns to Fig. 5, along with larger increases at higher global warming levels. Compared to the AMS, the more extreme 30-yr maximum metric shown in Fig. 5 is more relevant to typical long-lived infrastructure design applications. These results indicate the need to accommodate potentially larger future increases for the rarer events. Seneviratne et al. (2021) also show global average values of the change in 10-yr and 50-yr average recurrence intervals as a function of global warming level. These indicate somewhat larger changes for the 50-yr interval compared to the 10-yr interval.

GCM datasets typically are characterized by biases in precipitation (Pierce et al., 2023). Statistically downscaled methods remove much of the bias and produce datasets with statistical characteristics closer to observations. Statistical downscaling generates local-scale climate variations and should also reproduce the large-scale signal from the driving GCMs. However, projections of future values in the downscaled datasets are not necessarily constrained by historical observations. This raises the question: How do the large-scale patterns of future changes in precipitation extremes compare

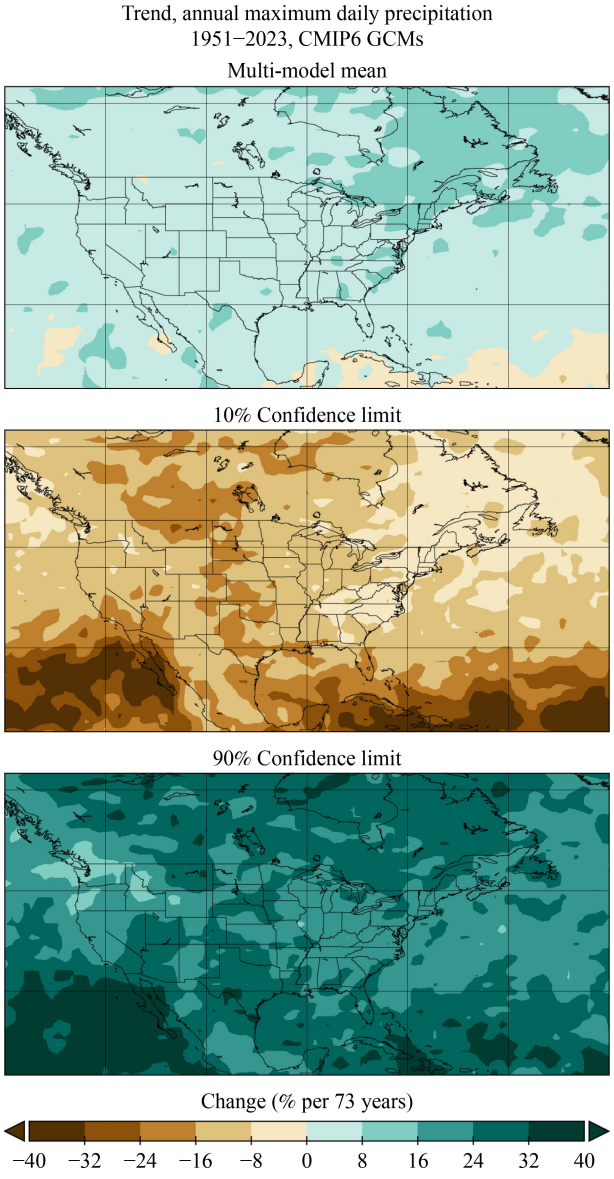

Fig. 3 Magnitude of the multi-model mean trend in Annual Maximum Series for 1951–2023 from 37 CMIP6 GCMs over the coterminous US and adjacent regions, in units of percent change over the 73-yr period of analysis. Panels are (top) mean, (middle) 10% confidence limit, and (bottom) 90% confidence limit.

between the downscaled datasets and the driving GCMs? Figure 6 illustrates the comparison of large-scale patterns of relative change from a historical period (1985–2014) to a future period (2070–2099) for the SSP5-8.5 scenario between the regridded LOCA2 and STAR downscaled datasets (Fig. 6, top panel) and the driving GCMs (Fig. 6, bottom panel). The large-scale patterns of future changes in the driving GCMs are reproduced in the downscaled datasets, indicating that the downscaled datasets largely retain the large-scale signal from the driving GCMs.

The non-stationary GEV method outlined in Section 2 (Eqs. (1)–(5)) was applied to the grid point data from the LOCA2 and STAR for a common set of 16 models. The percentage change in the daily duration threshold value for AEP = 0.5 and AEP = 0.01 was calculated for GWLs of 2°C and 4°C with respect to a GWL of 1.3°C, which approximates the near present level; this represents further warming of 0.7°C and 2.7°C, respectively. These percentage changes are hereafter referred to as "adjustment factors" (AFs). Figures 7 and 8 show the spatial patterns of AF for 2°C and 4°C GWL, respectively. The multi-model mean average is shown separately for the LOCA2 and STAR datasets. Several features are evident. One, the AFs are positive everywhere for both AEP levels, both GWL values, and both datasets. Second, the values for AEP = 0.01 are higher than for AEP = 0.5. Third, the values for STAR are somewhat higher than for LOCA2. Fourth, there are some differences in the spatial patterns between LOCA2 and STAR, most evident in the 4°C results (Fig. 8). Specifically, the increases are greater in the western US in STAR, with smaller differences elsewhere. An investigation of the source(s) of the differences between the two statistically-downscaled datasets was beyond the scope of this study, but they do illustrate that structural differences are present. The use of multiple datasets provides a means of incorporating this source of uncertainty in estimates of future change.

Dynamical downscaling can add new physics. However, such simulations are much more computationally intensive and thus the number and length of simulations is limited. On the other hand, statistical downscaling datasets are generally limited to daily durations. Datasets from dynamical downscaling simulations generally provide higher time resolution and are useful for examining the changes of sub-daily durations. We used the 7 NA-CORDEX models to investigate the relationship of relative adjustment factors between 24-h and 1-h durations. For each model grid point, the non-stationary GEV analysis described in Section 2 was applied to the AMS (Schlef et al., 2023). We then estimated the AFs of precipitation threshold for the 0.5 and 0.01 AEPs at the 4°C GWLs for 24-h and 1-h durations and calculated the ratio between the two durations. Figure 9 compares the results for 1-h duration with those for the 24-h duration. In general, the relative changes for the 1-h duration are modestly higher than the changes for the 24-h duration.

The results of the non-stationary GEV analyses, with GWL as the covariate, of the LOCA2, STAR, and NA-CORDEX datasets were used to produce summarized (CONUS averages) information for selected values of AEP and GWL. The summarized information for daily duration is shown in Table 3. This table includes AFs for GWLs of 2°C, 3°C, and 4°C, and for AEP values of 0.5, 0.2, 0.1, 0.04, 0.02, and 0.01. Adjustment factors increase with decreasing AEP for all three model datasets. The STAR AFs are larger than the LOCA2 AFs by 20%–30%, while the NA-CORDEX AFs are larger than the STAR

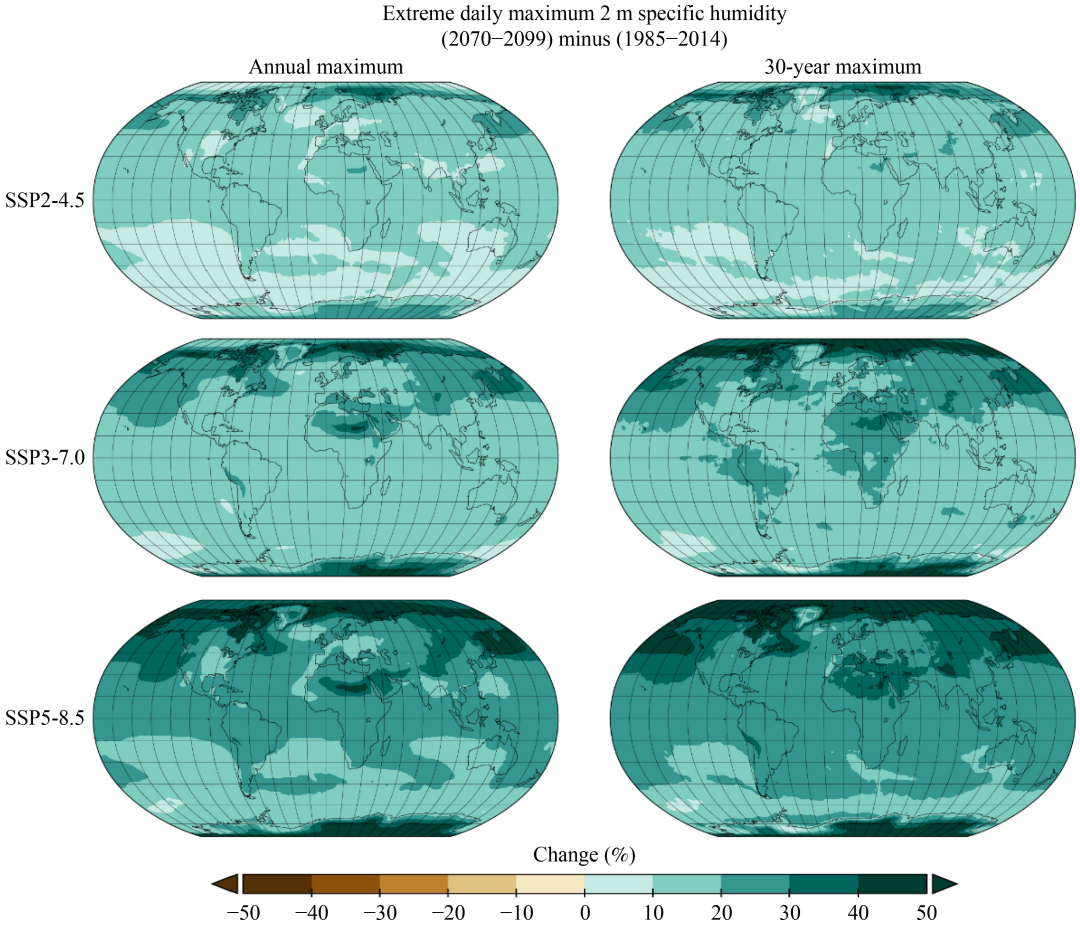

Fig. 4 Multi-model mean change (%) in extreme daily 2 m specific humidity for 2070–2099 relative to 1985–2014 for three emissions scenarios—SSP2-4.5 (top row, 31 models), SSP3-7.0 (middle row, 26 models), SSP5-8.5 (bottom row, 30 models)—and for the annual maximum daily 2 m specific humidity (left column) and 30-yr maximum daily 2m specific humidity (right column).

values by 10%–15%. The 90% confidence intervals are calculated from the multi-model standard deviation of the individual model AFs.

Table 4 shows similar values for 10-day duration. In all cases, the AFs are smaller than for the 1-day duration. The differences among the different model datasets are similar to the 1-day duration with AFs being smallest for LOCA2 and largest for NA-CORDEX.

Due to data availability limitations, AFs were only calculated from NA-CORDEX for the hourly duration (shown in Table 6). Then, the ratios between hourly and daily AFs are calculated and shown in Table 5, where hourly AFs are 26%–31% higher than the daily AFs. Further, these ratios were applied to the daily AFs for LOCA2 and STAR from Table 3 to provide estimated hourly AFs as follows:

$$\mathrm{AF}(\mathrm{hr},\mathrm{model}) = \mathrm{AF}(\mathrm{day},\mathrm{model}) \times \frac{\mathrm{AF}(\mathrm{hour},\mathrm{NACORDEX})}{\mathrm{AF}(\mathrm{day},\mathrm{NACORDEX})}. \quad (6)$$

This procedure ensures that the resulting hourly AF values for STAR and LOCA2 are internally consistent with their daily AFs. This approach provides consistency across durations by utilizing the large ensemble size of the LOCA2 and STAR data at daily resolution as the baseline. The information from the dynamically-downscaled ensemble provides physically-based information to extend the baseline daily adjustment factors to the hourly duration. These estimated values for LOCA2 and STAR are shown in Table 6. Since the relative changes from NA-CORDEX are applied directly to the STAR and LOCA2 data, the ranking of adjustment factors is the same as in Table 3.

5 Discussion and conclusions

The scientific basis for confidence in increases in extreme precipitation in most regions as the globe warms is primarily based on the direct effect of the dependence of AWVC on temperature and has been known for decades (e.g., IPCC, 1995; NAST, 2000). The quantitative magnitude of scaling with temperature is not settled and remains a topic of active research. The use of historical observations alone, and assuming a stationary climate, to estimate design values for extreme precipitation puts

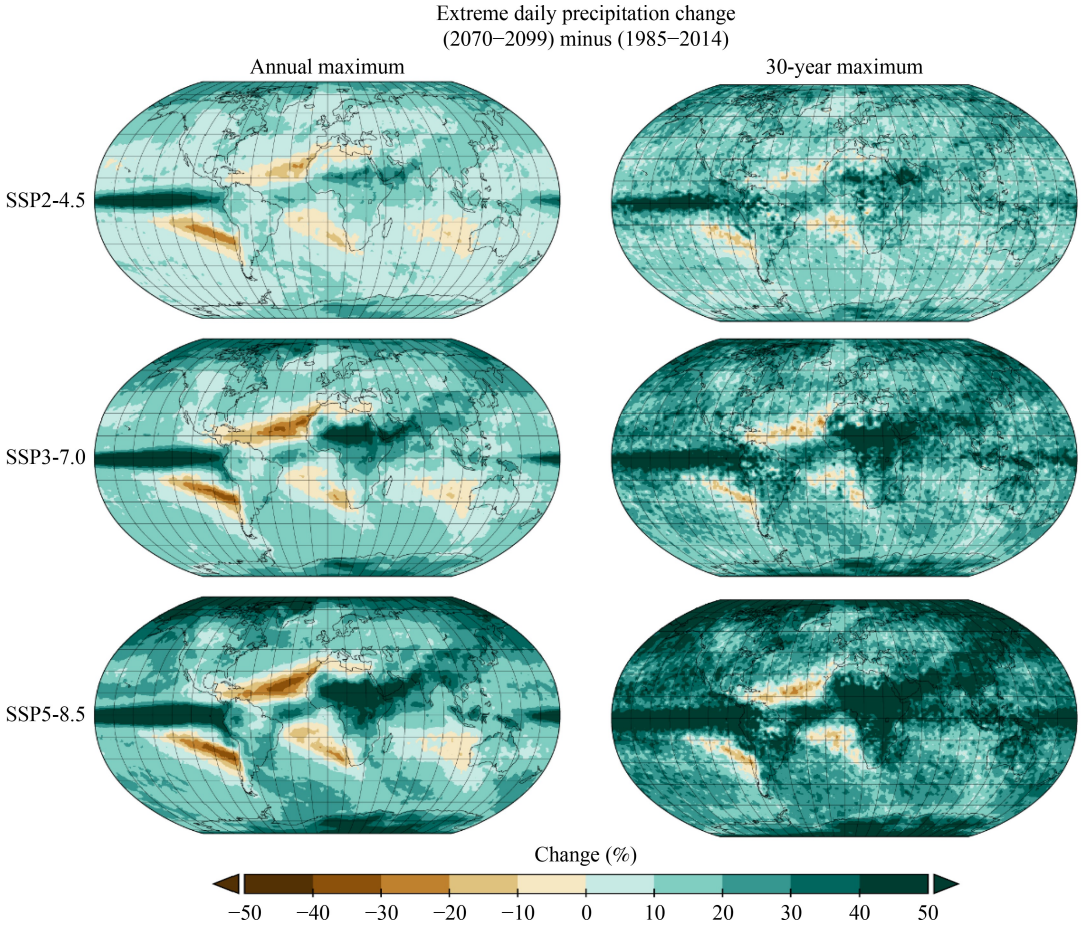

Fig. 5 Multi-model mean change (%) in extreme daily precipitation for 2070–2099 relative to 1985–2014 for three emissions scenarios: SSP2-4.5 (top row, 35 models), SSP3-7.0 (middle row, 31 models), SSP5-8.5 (bottom row, 37 models) and for the annual maximum daily precipitation (left column) and 30-yr maximum daily precipitation (right column).

long-lived infrastructure at increased risk of failure.

National and regional analyses of trends in extreme precipitation over CONUS generally show upward trends, consistent with the expected climate system response to warming. However, at the local scale, there are stations that show downward trends, although the large majority of stations with statistically significant trends show upward trends. This can raise a question to users about the need to incorporate potential future climate change into their planning and design for such locations. However, analysis of the CMIP6 GCMs shows a mix of upward and downward trends at the grid point level, even though the multi-model mean is uniformly positive. Thus, this mix of upward and downward trends in the historical observations, weighted toward upward trends, appears to be an expected aspect of climate system behavior, arising presumably from natural variability and sampling uncertainties superimposed on the signal from anthropogenic forcing. Natural variations and sampling variability are likely to be unpredictable on scales of decades, with anthropogenic forcing being the only factor with an unambiguous sign of change. This situation does represent a communication challenge. Schlef et al. (2023) summarize findings that in the short term the anthropogenic signal may be overwhelmed by natural variations. Thus, for short-term applications, extrapolation of historical trends may be justified.

Our analysis of the global and downscaled model data are consistent with other studies and provides an overarching framework for incorporating future change into rainfall design values for CONUS. The changes are larger for the higher emissions scenarios and higher global warming levels. Changes are also larger for rarer events and for shorter durations. We provide herein quantitative adjustment factors for CONUS based on these model analyses. These adjustment factors are meant to be applied to return level thresholds calculated from observed data. The basic framework for daily and longer durations is derived from the two statistically-downscaled datasets used in the Fifth US National Climate Assessment (Basile et al., 2023): STAR and LOCA2. Both of these datasets, using modern downscaling methods, model the high tail of the daily precipitation distribution function with a high degree of fidelity compared to previous methods. They are thus suitable candidates for this application. While the adjustment

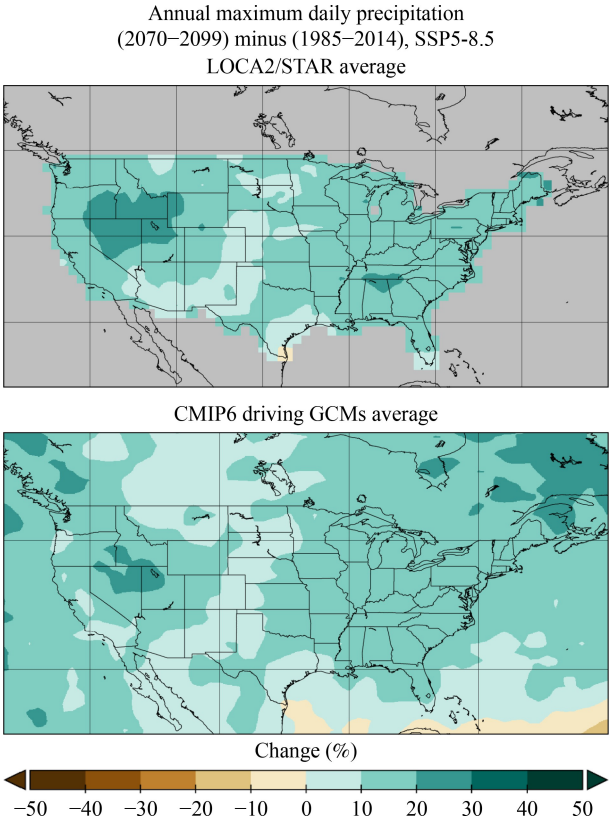

Fig. 6 Future change (%) for 2070–2099 in annual maximum daily precipitation relative to 1985–2014 under the SSP5-8.5 emissions scenario. Top panel is the average of 15 models from the LOCA2 and STAR downscaling datasets. Bottom panel is the average of the raw data from those same 15 models.

factors for LOCA2 and STAR are similar, they are not identical with STAR values generally a little larger than the LOCA2 values. The use of adjustment factors from both datasets introduces a dimension of structural uncertainty, increasing the comprehensiveness of uncertainty consideration. An extension to hourly duration is achieved through relative adjustments to the daily duration adjustment factors from an analysis of NA-CORDEX data.

These adjustment factors were calculated for GWLs relative to the level of global warming achieved to the present time of 1.3°C. Thus, they are most appropriately applied to values calculated from historical observations that have been updated to include the most recent observations, ideally using non-stationary statistical methods.

The adjustment from daily to hourly durations used herein is about a factor of 1.3. Short durations pose a particular challenge for estimation of adjustment factors for at least two reasons. First, there are few climate models simulations with available hourly and sub-hourly data. The NA-CORDEX is a prime source of such data and we used these data for quantitative guidance with respect to the relationship between daily changes and hourly changes. Second, at shorter durations, the effects of individual convective cells on precipitation frequencies likely becomes more important. While the NA-CORDEX simulations are at a high spatial resolution (25 km) compared to typical global models, they do not simulate individual cells. A class of models, denoted as

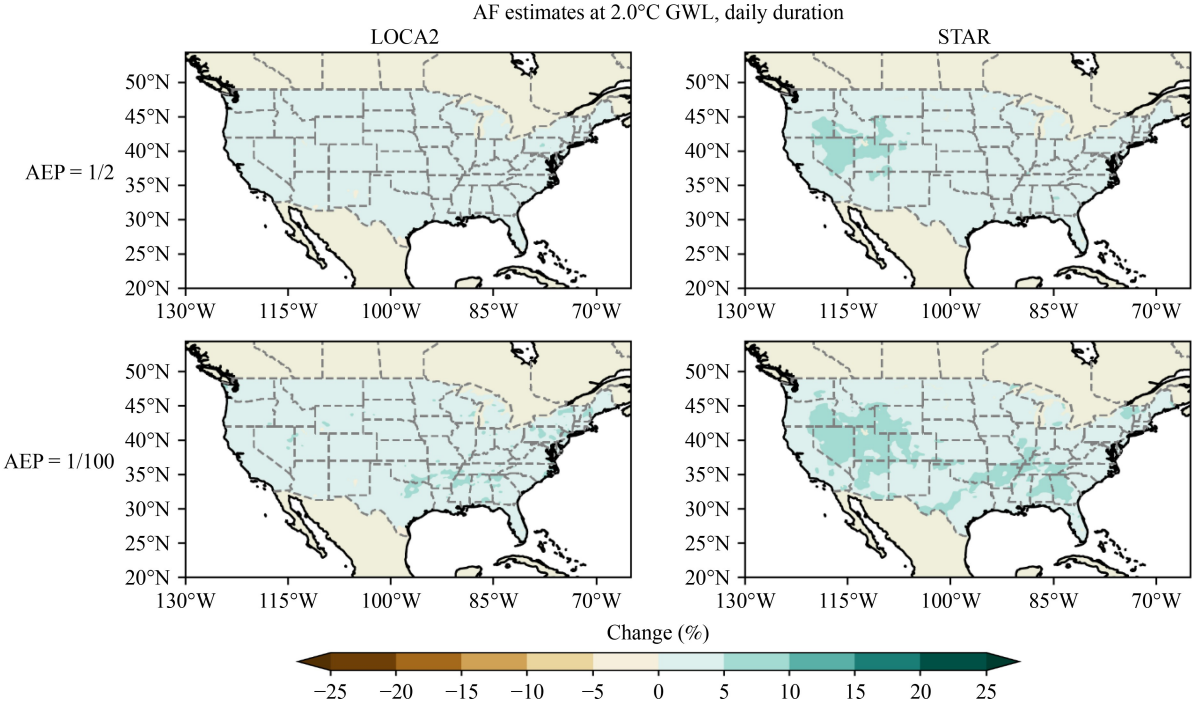

Fig. 7 Multi-model (16 models) average of the adjustment factor (%) in the daily duration threshold for AEP = 0.5 (top panels) and AEP = 0.01 (bottom panels) and for LOCA2 (left panels) and STAR (right panels). Results are for the 2°C GWL with respect to the 2024 global warming level of 1.3°C.

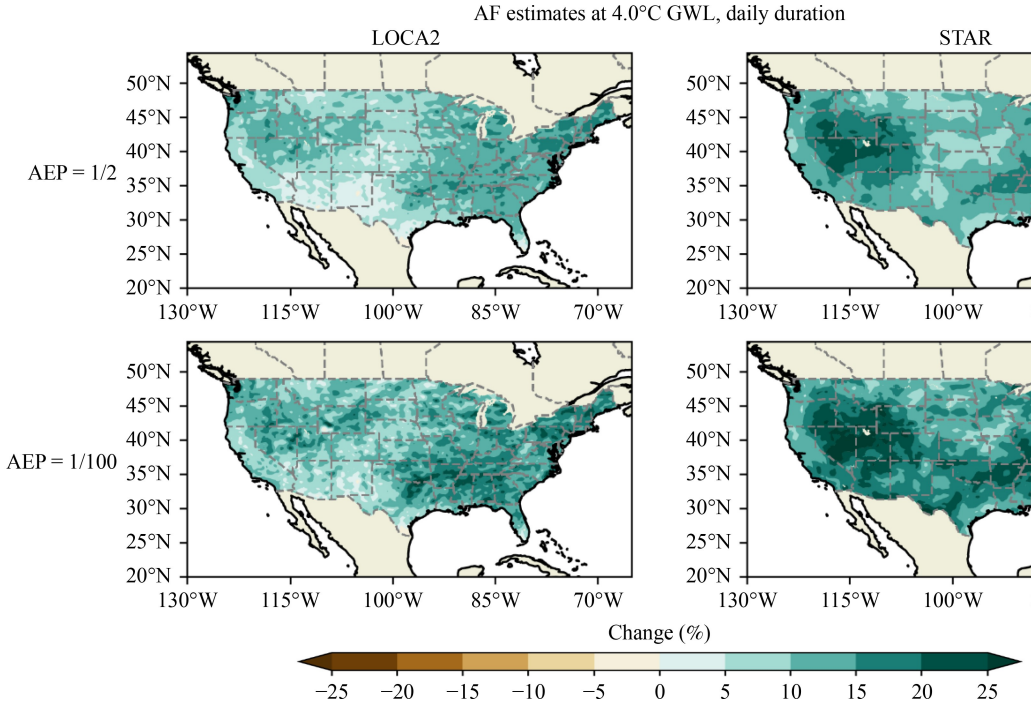

Fig. 8 Same as Fig. 7 except for the GWL level of 4°C relative to the 2024 GWL of 1.3°C.

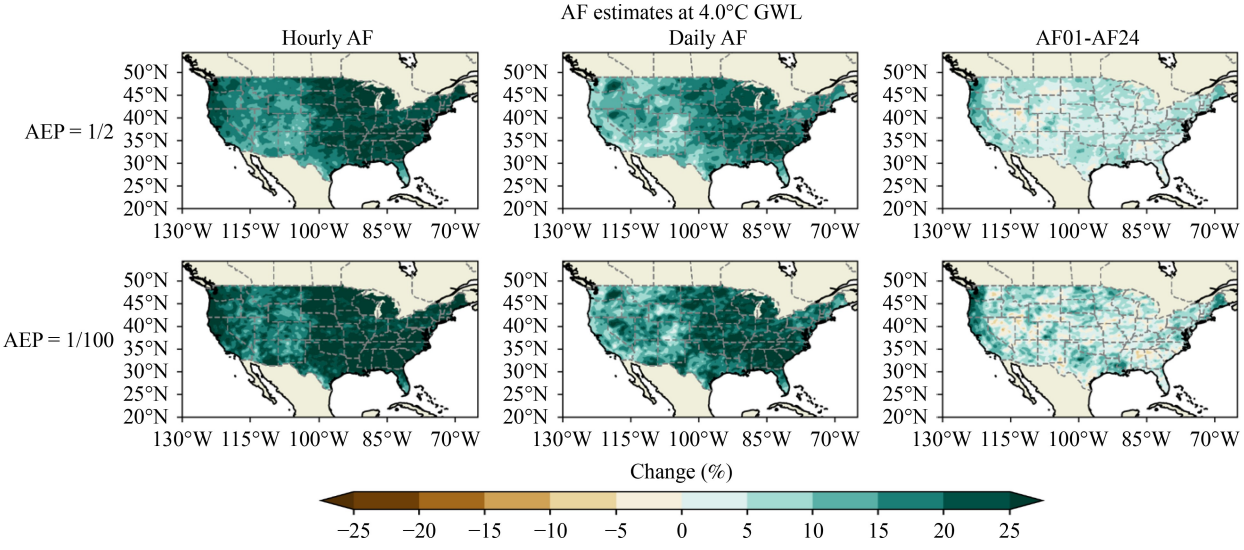

Fig. 9 Multi-model mean adjustment factors (%) for AEP = 0.5 (top panels) and AEP = 0.01 (bottom panels) from the 7 NA-CORDEX models. Results include the relative change at the 4°C GWL relative to the value at 1.3°C GWL for the 1-h duration (left panels), the 24-h duration (middle panels), and the differences, hourly minus daily (right panels).

convection-permitting models (CPMs), do resolve such cells. For example, the CONUS404 dataset (Rasmussen et al., 2023) is a 42-yr long simulation of the recent historical period (1979–2021). This simulation is at a convection-permitting spatial resolution of 4 km. Because of the massive computational resources required to run such models for multi-decadal time periods, the number and length of such simulations is very limited at the present time. As CPM data resources increase, they will provide firmer physical insights into the effects of global warming on extreme precipitation.

Acknowledgments We acknowledge the World Climate Research Programme, which, through its Working Group on Coupled Modeling, coordinated and promoted CMIP6. We thank the climate modeling groups for producing and making available their model output. This research was supported by the National Oceanic and Atmospheric Administration through the Cooperative Institute for Satellite Earth System Studies under Cooperative Agreement NA19NES4320002, the Cooperative Institute for Research to Operations in Hydrology in cooperation with RTI International under Cooperative Agreement NA23NWS4050004I and by National Science Foundation (NSF) award No. 2221803. The statements, findings, conclusions, and recommendations are those of the author(s) and do not necessarily reflect the views of NOAA and NSF.

Table 3 CONUS-averaged adjustment factors (in bold) with 90% confidence intervals (in parenthesis) for the daily duration for three datasets: STAR, LOCA2 and NA-CORDEX at three global warming levels (GWL)

GWL	Datasets	AEP					
		1/2	1/5	1/10	1/25	1/50	1/100
2°C	STAR	**3.5**	**3.7**	**3.9**	**4.0**	**4.1**	**4.2**
		(2.1, 4.9)	(2.2, 5.2)	(2.3, 5.4)	(2.3, 5.7)	(2.4, 5.8)	(2.4, 5.9)
	LOCA2	**2.5**	**2.7**	**2.8**	**2.9**	**3.0**	**3.0**
		(1.4, 3.7)	(1.5, 4.0)	(1.5, 4.1)	(1.5, 4.3)	(1.5, 4.4)	(1.5, 4.5)
	NA-CORDEX	**3.5**	**3.6**	**3.7**	**3.8**	**3.9**	**4.0**
		(2.1, 4.8)	(2.1, 5.2)	(2.1, 5.4)	(2.1, 5.6)	(2.0, 5.8)	(2.0, 5.9)
3°C	STAR	**8.4**	**9.0**	**9.4**	**9.8**	**10.0**	**10.2**
		(5.7, 11.0)	(6.0, 12.0)	(6.2, 12.6)	(6.3, 13.2)	(6.4, 13.6)	(6.4, 13.9)
	LOCA2	**6.1**	**6.6**	**6.8**	**7.1**	**7.2**	**7.4**
		(3.8, 8.4)	(4.0, 9.1)	(4.1, 9.5)	(4.2, 10.0)	(4.2, 10.2)	(4.3, 10.4)
	NA-CORDEX	**9.5**	**10.0**	**10.4**	**10.7**	**10.9**	**11.0**
		(6.4, 12.5)	(6.5, 13.6)	(6.5, 14.3)	(6.4, 15.0)	(6.4, 15.4)	(6.3, 15.8)
4°C	STAR	**13.4**	**14.6**	**15.3**	**16.0**	**16.4**	**16.7**
		(9.2, 17.5)	(9.9, 19.3)	(10.2, 20.4)	(10.5, 21.5)	(10.6, 22.1)	(10.7, 22.7)
	LOCA2	**9.7**	**10.6**	**11.0**	**11.5**	**11.8**	**12.0**
		(6.2, 13.3)	(6.6, 14.6)	(6.8, 15.3)	(6.9, 16.1)	(7.0, 16.6)	(7.1, 17.0)
	NA-CORDEX	**15.6**	**16.8**	**17.4**	**18.0**	**18.4**	**18.8**
		(10.7, 20.6)	(10.8, 22.7)	(10.8, 23.9)	(10.8, 25.3)	(10.7, 26.1)	(10.7, 26.8)

Table 4 Similar to Table 3, but for 10-day duration

GWL	Datasets	AEP					
		1/2	1/5	1/10	1/25	1/50	1/100
2°C	STAR	**2.7**	**2.9**	**3.0**	**3.0**	**3.1**	**3.2**
		(1.4, 4.0)	(1.5, 4.2)	(1.6, 4.4)	(1.6, 4.5)	(1.6, 4.6)	(1.6, 4.7)
	LOCA2	**2.0**	**2.2**	**2.2**	**2.3**	**2.4**	**2.4**
		(0.9, 3.1)	(1.0, 3.3)	(1.0, 3.5)	(1.1, 3.6)	(1.1, 3.7)	(1.1, 3.8)
	NA-CORDEX	**2.4**	**2.6**	**2.6**	**2.7**	**2.8**	**2.8**
		(1.2, 3.7)	(1.2, 3.9)	(1.2, 4.1)	(1.2, 4.2)	(1.2, 4.4)	(1.1, 4.5)
3°C	STAR	**6.6**	**7.0**	**7.2**	**7.5**	**7.6**	**7.7**
		(4.0, 9.2)	(4.2, 9.8)	(4.3, 10.2)	(4.4, 10.6)	(4.4, 10.9)	(4.4, 11.1)
	LOCA2	**4.8**	**5.3**	**5.5**	**5.8**	**5.9**	**6.0**
		(2.6, 7.1)	(2.9, 7.7)	(3.0, 8.1)	(3.1, 8.4)	(3.2, 8.7)	(3.2, 8.9)
	NA-CORDEX	**6.7**	**7.1**	**7.4**	**7.6**	**7.8**	**7.9**
		(3.8, 9.6)	(3.9, 10.3)	(3.9, 10.8)	(3.9, 11.4)	(3.8, 11.7)	(3.8, 12.0)
4°C	STAR	**10.6**	**11.4**	**11.8**	**12.2**	**12.5**	**12.7**
		(6.5, 14.6)	(7.0, 15.8)	(7.1, 16.5)	(7.2, 17.2)	(7.3, 17.6)	(7.3, 18.0)
	LOCA2	**7.8**	**8.6**	**9.0**	**9.4**	**9.7**	**9.9**
		(4.3, 11.2)	(4.8, 12.3)	(5.0, 13.0)	(5.2, 13.6)	(5.3, 14.0)	(5.4, 14.4)
	NA-CORDEX	**11.1**	**11.9**	**12.3**	**12.8**	**13.1**	**13.4**
		(6.4, 15.7)	(6.6, 17.1)	(6.6, 18.1)	(6.6, 19.1)	(6.5, 19.7)	(6.5, 20.3)

Table 5 Ratios of the AFs between hourly and daily durations for the NA-CORDEX dataset

GWL	AEP					
	1/2	1/5	1/10	1/25	1/50	1/100
2°C	1.29	1.28	1.27	1.26	1.26	1.25
3°C	1.30	1.30	1.29	1.29	1.29	1.29
4°C	1.31	1.31	1.30	1.30	1.30	1.30

Table 6 Similar to Table 3, but for hourly duration. Estimated values for LOCA2 and STAR datasets are italicized

GWL	Datasets	AEP					
		1/2	1/5	1/10	1/25	1/50	1/100
2°C	STAR	**4.5** (2.8, 6.3)	**4.8** (2.9, 6.7)	**4.9** (2.9, 6.9)	**5.0** (3.0, 7.2)	**5.1** (3.0, 7.3)	**5.2** (3.0, 7.4)
	LOCA2	**3.3** (1.8, 4.7)	**3.4** (1.9, 5.0)	**3.6** (1.9, 5.2)	**3.6** (1.9, 5.4)	**3.7** (1.9, 5.5)	**3.8** (1.9, 5.6)
	NA-CORDEX	**4.5** (3.0, 6.0)	**4.6** (3.0, 6.3)	**4.8** (3.0, 6.5)	**4.8** (3.0, 6.7)	**4.9** (2.9, 6.9)	**5.0** (2.9, 7.0)
3°C	STAR	**10.9** (7.4, 14.4)	**11.7** (7.8, 15.6)	**12.1** (8.0, 16.3)	**12.6** (8.1, 17.0)	**12.8** (8.2, 17.5)	**13.0** (8.3, 17.8)
	LOCA2	**7.9** (4.9, 10.9)	**8.5** (5.2, 11.8)	**8.8** (5.3, 12.3)	**9.1** (5.4, 12.8)	**9.3** (5.4, 13.2)	**9.4** (5.5, 13.4)
	NA-CORDEX	**12.3** (8.9, 15.8)	**13.0** (9.0, 17.1)	**13.4** (8.9, 17.8)	**13.8** (8.9, 18.6)	**14.0** (8.9, 19.1)	**14.2** (8.8, 19.6)
4°C	STAR	**17.50** (12.1, 22.9)	**19.06** (12.9, 25.2)	**19.92** (13.3, 26.6)	**20.78** (13.6, 28.0)	**21.29** (13.8, 28.8)	**21.70** (13.9, 29.5)
	LOCA2	**12.71** (8.0, 17.4)	**13.79** (8.6, 19.0)	**14.39** (8.8, 20.0)	**14.98** (9.0, 20.9)	**15.34** (9.1, 21.5)	**15.63** (9.2, 22.0)
	NA-CORDEX	**20.5** (14.7, 26.3)	**21.9** (14.9, 28.8)	**22.6** (14.9, 30.4)	**23.5** (14.9, 32.0)	**24.0** (14.9, 33.0)	**24.4** (14.9, 33.8)

Competing interests The authors declare that they have no competing interests.

References

Basile S, Crimmins A R, Avery C W, Hamlington B D, Kunkel K E (2023). Appendix 3. Scenarios and datasets. In: Fifth National Climate Assessment. Crimmins A R, Avery C W, Easterling D R, Kunkel K E, Stewart B C, and Maycock T K, Eds. U. S. Global Change Research Program, Washington, DC, USA

Bonnin G M, Martin D, Lin B, Parzybok T, Yekta M, Riley D (2006a). NOAA Atlas 14 Precipitation-Frequency Atlas of the United States Volume 1 Version 4.0: Semiarid Southwest (Arizona, Southeast California, Nevada, New Mexico, Utah). Technical Report, U.S. Department of Commerce, National Oceanic and Atmospheric Administration, National Weather Service, Maryland: Silver Spring

Bonnin G M, Martin D, Lin B, Parzybok T, Yekta M, Riley D (2006b). NOAA Atlas 14 Precipitation-Frequency Atlas of the United States Volume 2 Version 3.0: Delaware, District of Columbia, Illinois, Indiana, Kentucky, Maryland, New Jersey, North Carolina, Ohio, Pennsylvania, South Carolina, Tennessee, Virginia, West Virginia. Technical Report, U.S. Department of Commerce, National Oceanic and Atmospheric Administration, National Weather Service, Maryland: Silver Spring

Bonnin G M, Martin D, Lin B, Parzybok T, Yekta M, Riley D (2006c). NOAA Atlas 14 Precipitation-Frequency Atlas of the United States Volume 3 Version 3.0: Puerto Rico and the U.S. Virgin Islands. Technical Report, U.S. Department of Commerce, National Oceanic and Atmospheric Administration, National Weather Service, Maryland: Silver Spring

DeGaetano A T, Castellano C M (2017). Future projections of extreme precipitation intensity-duration- frequency curves for climate adaptation planning in New York State. Clim Serv, 5: 23–35

Douville H, Raghavan K, Renwick J, Allan R P, Arias P A, Barlow M, Cerezo-Mota R, Cherchi A, Gan T Y, Gergis J, Jiang D, Khan A, Mba W P, Rosenfeld D, Tierney J, Zolina O (2021). Water Cycle Changes. In Climate Change 2021: The Physical Science Basis. Contribution of Working Group I to the Sixth Assessment Report of the Intergovernmental Panel on Climate Change [Masson-Delmotte V, Zhai P, Pirani A, Connors S L, Péan C, Berger S, Caud N, Chen Y, Goldfarb L, Gomis M I, Huang M, Leitzell K, Lonnoy E, Matthews J B R, Maycock T K, Waterfield T, Yelekçi O, Yu R, and Zhou B (eds.)]. Cambridge University Press, Cambridge, United

Kingdom and New York, NY, USA, 1055–1210.

Eyring V, Bony S, Meehl G A, Senior C A, Stevens B, Stouffer R J, Taylor K E (2016). Overview of the coupled model intercomparison project phase 6 (CMIP6) experimental design and organization. Geosci Model Dev, 9(5): 1937–1958

Förster K, Thiele L B (2020). Variations in sub-daily precipitation at centennial scale. NPJ Climate and Atmospheric Science, 3: 13

Hayhoe K, Scott-Fleming I Stoner A, Wuebbles D (2024). STAR-ESDM: a generalizable approach to generating high-resolution climate projections through signal decomposition. Earth's Future, 12: e2023EF004107

Holton J R (1992). An Introduction to Dynamic Meteorology, 3rd Ed. New York: Academic Press

IPCC (1995). Climate Change 1995: A Report of the Intergovernmental Panel on Climate Change (Cambridge, United Kingdom and New York, NY, USA: Cambridge University Press)

IPCC (2021). Climate Change 2021: The Physical Science Basis. Contribution of Working Group I to the Sixth Assessment Report of the Intergovernmental Panel on Climate Change. Cambridge: Cambridge University Press

Kunkel K E, Easterling D R, Kristovich D A R, Gleason B, Stoecker L, Smith R (2012). Meteorological causes of the secular variations in observed extreme precipitation events for the conterminous United States. J Hydrometeorol, 13(3): 1131–1141

Kunkel K E, Karl T R, Squires M F, Yin X, Stegall S T, Easterling D R (2020a). Precipitation extremes: trends and relationships with average precipitation and precipitable water in the contiguous united states. J Appl Meteorol Climatol, 59(1): 125–142

Kunkel K E, Stevens S E, Stevens L E, Karl T R (2020b). Observed climatological relationships of extreme daily precipitation events with precipitable water and vertical velocity in the Contiguous United States. Geophys Res Lett, 47(12): e2019GL086721

Li C, Zwiers F, Zhang X, Chen G, Lu J, Li G, Norris J, Tan Y, Sun Y, Liu M (2019). Larger increases in more extreme local precipitation events as climate warms. Geophys Res Lett, 46(12): 6885–6891

Marvel K, Su W, Delgado R, Aarons S, Chatterjee A, Garcia M E, Hausfather Z, Hayhoe K, Hence D A, Jewett E B, Robel A, Singh D, Tripati A, Vose R S (2023). Ch. 2. Climate trends. In: Crimmins A R, Avery C W, Easterling D R, Kunkel K E, Stewart B C, and Maycock T K, eds. Fifth National Climate Assessment U. S. Global Change Research Program, Washington, DC, USA

NASEM (National Academies of Sciences, Engineering, and Medicine) (2024). Modernizing Probable Maximum Precipitation Estimation. Washington, DC: The National Academies Press

NAST (2000). Climate Change Impacts on the United States: The Potential Consequences of Climate Variability and Change. In: Report for the US Global Change Research Program, Cambridge: Cambridge University Press

Nazarian R H, Vizzard J V, Agostino C P, Lutsko N J (2022). Projected changes in future extreme precipitation over the Northeast United States in the NA-CORDEX ensembles. J Appl Meteorol Climatol, 61(11): 1649–1668

Neelin J D, Martinez-Villalobos C, Stechmann S N, Ahmed F, Chen G, Norris J M, Kuo Y H, Lenderink G (2022). Precipitation extremes and water vapor: relationships in current climate and implications for climate change. Curr Clim Change Rep, 8(1): 17–33

O'Gorman P A (2015). Precipitation extremes under climate change. Curr Clim Change Rep, 1(2): 49–59

O'Gorman P A, Schneider T (2009). The physical basis for increases in precipitation extremes in simulations of 21st-century climate change. Proc Natl Acad Sci USA, 106(35): 14773–14777

O'Neill B C, Tebaldi C, van Vuuren D P, Eyring V, Friedlingstein P, Hurtt G, Knutti R, Kriegler E, Lamarque J F, Lowe J, Meehl G A, Moss R, Riahi K, Sanderson B M (2016). The scenario model intercomparison project (ScenarioMIP) for CMIP6. Geosci Model Dev, 9(9): 3461–3482

OWP (2022). Analysis of Impact of Nonstationary Climate on NOAA Atlas 14 Estimates. Technical Report, National Weather Service, Office of Water Prediction

Pierce D W, Cayan D R, Feldman D R, Risser M D (2023). Future increases in North American extreme precipitation in CMIP6 downscaled with LOCA. J Hydrometeorol, 24(5): 951–975

Prein A, Rasmussen R, Ikeda K, Liu C, Clark M P, Holland G J (2017). The future intensification of hourly precipitation extremes. Nat Clim Chang, 7(1): 48–52

Rasmussen R M, Chen F, Liu C, Ikeda K, Prein A, Kim J, Schneider T, Dai A, Gochis D, Dugger A, Zhang Y, Jaye A, Dudhia J, He C, Harrold M, Xue L, Chen S, Newman A, Dougherty E, Abolafia-Rosenzweig R, Lybarger N D, Viger R, Lesmes D, Skalak K, Brakebill J, Cline D, Dunne K, Rasmussen K, Miguez-Macho G (2023). CONUS404: The NCAR–USGS 4-km long-term regional hydroclimate reanalysis over the CONUS. Bull Am Meteorol Soc, 104(8): E1382–E1408

Schlef K E, Kunkel K E, Brown C, Demissie Y, Lettenmaier D P, Wagner A, Wigmosta M S, Karl T R, Easterling D R, Wang K J, Francois B, Yan E (2023). Incorporating non-stationarity from climate change into rainfall frequency and intensity-duration-frequency (IDF) curves. J Hydrol (Amst), 616: 128757

Seneviratne S I, Zhang X, Adnan M, Badi W, Dereczynski C, Di Luca A, Ghosh S, Iskander I, Kossin J, Lewis S, Otto F, Pinto I, Satoh M, Vicente-Serrano S M, Wehner M, Zhou B (2021). Weather and Climate Extreme Events in a Changing Climate (Chapter 11). In: IPCC 2021: Climate Change 2021: The Physical Science Basis. Contribution of Working Group I to the Sixth Assessment Report of the Intergovernmental Panel on Climate Change. [Masson-Delmotte V, Zhai P, Pirani A, Connors S L, Péan C, Berger S, Caud N, Chen Y, Goldfarb L, Gomis M I, Huang M, Leitzell K, Lonnoy E, Matthews J B R, Maycock T K, Waterfield T, Yelekçi O, Yu R, and Zhou B (eds.). Cambridge, United Kingdom and New York, NY, USA: Cambridge University Press, 1513–1766

USGCRP (2023). Fifth National Climate Assessment. In: U.S. Global Change Research Program. Washington, DC, USA

Wilks D S (2016). "The stippling shows statistically significant grid points": How research results are routinely overstated and overinterpreted, and what to do about it. Bull Am Meteorol Soc, 97(12): 2263–2273

Wright D B, Bosma C D, Lopez-Cantu T (2019). U. S. hydrologic design standards insufficient due to large increases in frequency of rainfall extremes. Geophys Res Lett, 46(14): 8144–8153

Wright D B, Samaras C, Lopez-Cantu T (2021). Resilience to extreme rainfall starts with science. Bull Am Meteorol Soc, 102(4): E808–E813